Magnetotransport in multiple narrow silicon inversion channels opened electrostatically into a two-dimensional electron gas

Philip F. Bagwell*
Department of Electrical Engineering and Computer Science, Massachusetts Institute of Technology, Cambridge, Massachusetts 02139

Samuel L. Park†
Department of Physics, Massachusetts Institute of Technology, Cambridge, Massachusetts 02139

Anthony Yen,‡ Dimitri A. Antoniadis, Henry I. Smith, and T.P. Orlando
Department of Electrical Engineering and Computer Science, Massachusetts Institute of Technology, Cambridge, Massachusetts 02139

Marc A. Kastner
Department of Physics, Massachusetts Institute of Technology, Cambridge, Massachusetts 02139
(Received 12 July 1991)

We study electrical transport in a dual-gate metal-oxide-semiconductor field-effect transistor. The bottom gate is a grating which allows the inversion-layer geometry to be controlled electrostatically. We compare the magnetoconductance of many parallel narrow-inversion channels, a modulated potential, and a uniform two-dimensional electron gas all formed in the same Si crystal. Electron weak localization becomes much more pronounced as the device is electrostatically pinched from a two-dimensional inversion layer into many narrow wires in parallel, proving that the wire width can be reduced below the electron phase coherence length. For magnetic fields greater than 1 T normal to the sample surface there is a large drop in the current, which persists to room temperature, as electrons are added to the device so that it opens electrostatically from many narrow inversion layers in parallel into a two-dimensional electron gas. This large negative transconductance results from electrostatically changing the dominant boundary condition on the classical Drude magnetoconductance tensor from that of a long and narrow to a short and wide conductor. Quantum edge states form at high magnetic fields, giving a high-field magnetoconductance of opposite sign for the parallel wires and wide electron gas. Thus, the evolution from Shubnikov–de Haas oscillations tc the quantum Hall effect depends strongly and qualitatively on the device aspect ratio. At a magnetic field of 30 T the two-terminal conductance versus gate voltage of the narrow wires evolves into quantum Hall steps having a height of $2e^2/h$ multiplied by the number of wires in parallel. In contrast to a wide device the conduction-band valley degeneracy is not resolved, giving rise to Hall steps of twice the expected size.

I. INTRODUCTION

The confinement of electrons to narrow Si inversion channels[1–5] can be achieved by means of dual gates incorporated into a metal-oxide-semiconductor field-effect transistor (MOSFET). Varying the two gate voltages controls both the electron density and the width of the narrow channel. A variety of conductance fluctuation phenomena,[6–9] weak localization,[10] Shubnikov–de Haas oscillations and their evolution into the quantum Hall effect,[11–14] and possible electron charging effects[4] have been demonstrated in narrow Si inversion layers. Although the mean free path in Si inversion layers is much shorter than in an electron gas formed at a $GaAs/Al_xGa_{1-x}As$ heterojunction, electrostatic control of the Si inversion-layer geometry is much easier using a MOS field-effect capacitor. We exploit field-effect control of the Si inversion-layer geometry to study in a single device the electrical conductance of an array of narrow wires, a modulated potential, and a two-dimensional electron gas as a function of electron density, magnetic field, and temperature.

Our device geometry is the dual gate MOSFET shown in Fig. 1. The bottom gate is a W grating gate having a 200-nm period, and is separated from the inversion channel by a 20-nm-thick SiO_2 insulating layer. All the grating lines are electrically connected at the bottom-gate contact pad. A further 500 nm of SiO_x separates the grating gate from a second continuous Al gate electrode. Standard MOSFET devices made with a continuous W gate on the same wafer had a mobility of 5000 cm^2/Vs at a temperature of 4.2 K. The device fabrication technology is described elsewhere.[3–5]

II. DEVICE CHARACTERISTICS

We measure the rms ac drain current I_{DS} of the MOSFET device of Fig. 1 at low rms ac drain voltage, $V_{DS} = 25\ \mu V$, using standard lock-in amplifier techniques. When the device is cooled to low temperature, $T \leq 50$ mK, in a dilution refrigerator, the conductance $G = I_{DS}/V_{DS}$ versus gate voltage in Fig. 2 is obtained. In Fig. 2 the top-gate voltage V_{TG} is swept from -16 V $\leq V_{TG} \leq 20$ V holding the grating gate voltage V_{BG} fixed at different values.

Figure 2 shows that, for the family of curves where $V_{BG} = 2.5$ V, 3 V, 4 V, and 5 V there is a clear "break" or "kink" in the device I-V around $V_{TG} \simeq 0$ V. For $V_{TG} \leq 0$ V on this family of curves the electron gas is confined only beneath the grating wires as in Fig. 1(a), while for $V_{TG} \geq 0$ V the electron gas exists everywhere in the channel. The "break" in the device I-V curves as the entire channel becomes inverted can be understood using a simple model where conduction both underneath the grating wires and in the gap between grating wires is viewed as two independent MOSFET's in parallel having different threshold voltages. When the grating gate V_{BG} is held well above its threshold voltage (approximately 1.2 V), negatively biasing the top gate can shut off the transistor current on this family of curves. This can only happen if electrostatic fringing fields around the bottom gate are significant, so that the field lines from the top gate can reach around the bottom gate and turn off the electron gas.

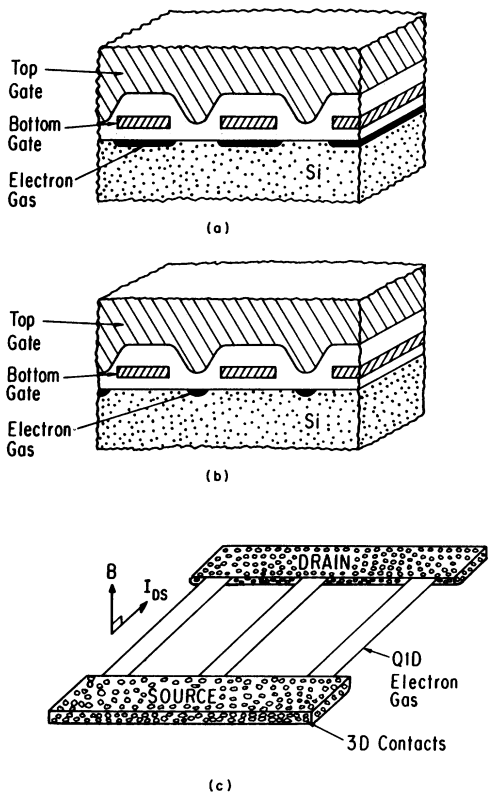

FIG. 1. "Grating gate" MOSFET geometry. The split gates permit control of the inversion-layer geometry via the field effect. A narrow inversion layer can form either (a) underneath the grating lines or (b) in the gap between the grating lines. A wide inversion layer having a modulated electron density can also be created by appropriately adjusting the two gate voltages. The complete inversion-layer geometry guiding the current flow, including the device contacts and the direction of the applied magnetic field, is shown in (c).

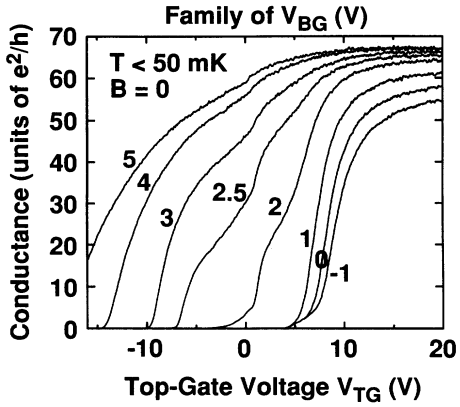

FIG. 2. Static device I-V for zero applied magnetic field. The five curves on the left show a pronounced "kink" near zero volts, indicating a transition where the inversion layer opens electrostatically from an array of narrow channels underneath the grating wires to a two-dimensional electron gas. The three rightmost curves, where no kink is observed, indicate the electron gas exists only in the gap between grating lines over the range of voltages shown.

For the family of bottom-gate voltages $V_{BG} = 1$ V, 0 V, and -1 V in Fig. 2 there is no "kink" or "break" in the I-V characteristics. For this family of curves the electron gas is confined only in the gap between grating lines as in Fig. 1(b). The entire MOSFET channel does not become inverted for this family of curves, as we subsequently prove by examining the device magnetoconductance.[15] The current saturates in Fig. 2 due to the 330-Ω resistance of the wires running into the dilution refrigerator in series with the 50-Ω device contact resistance. This same series resistance is present in Figs. 2–5, as the same device and measurement conditions are used in these figures.

We now establish an inversion layer by fixing the top-gate voltage at $V_{TG} = 13$ V and gradually pinch the electron gas down into narrow inversion strips using $V_{BG} = 3$ V, 1.5 V, 0 V, and -1.25 V (Fig. 3). The magnetic field B is swept from -1 T to 8 T. As the electron gas is pinched into narrow channels the zero-field conductance decreases as expected. However, as the bottom-gate voltage passes below its threshold from $V_{BG} = 1.5$ V to $V_{BG} = 0$ V, a large weak localization[16] magnetoresistance feature develops around $B = 0$ T. The development of this large weak localization feature proves that wires having a width W smaller than the electron phase coherence length L_ϕ are formed, and is further indication that narrow inversion channels are present.

Since the electron motion is diffusive, an applied magnetic field extinguishes weak localization when a few magnetic flux quanta ($\phi_0 = h/2e$) are enclosed by the average diffusion path to return to the origin. If this semiclassical

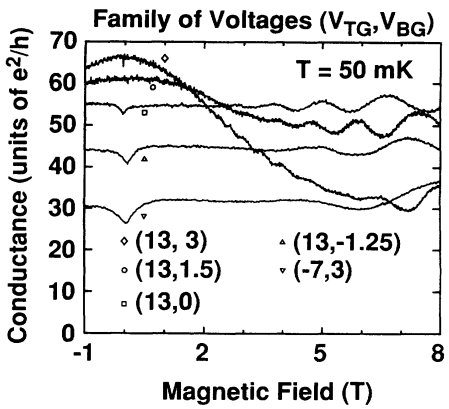

FIG. 3. A pronounced weak localization minimum develops around $B = 0$ T as the two-dimensional inversion layer is pinched into narrow wires, indicating that the wire width has become smaller than the electron phase coherence length. A corresponding qualitative change in the background Drude magnetoconductance also occurs as the device is pinched into multiple parallel narrow wires, so that the negative magnetoconductance of a wide electron gas is large but the magnetoconductance of the array of narrow wires is small. (The voltages V_{BG} and V_{TG} are given in volts.)

diffusion path is constrained by a boundary, such as the side of a narrow wire, then the area enclosed by the average diffusion path is much smaller. Therefore, a higher magnetic field is needed to turn off the weak localization in a narrow wire. This critical magnetic field B_c is approximately given by $B_c \simeq \phi_0/(L_\phi)^2$ in two dimensions, and increases to $B_c \simeq \phi_0/(WL_\phi)$ when the wire is narrow such that $W \leq L_\phi$. The size of the weak localization conductance correction is also much larger in one dimension than in two dimensions. Using the semiclassical one-dimensional weak localization formula of Al'tshuler and Aronov,[17] and after correcting for series resistance, we obtain an electron phase coherence length $L_\phi \simeq 0.6$ μm and a wire width $W \simeq 350$–450 Å when $V_{BG} = 0$ V and $V_{TG} = 13$ V in Fig. 3. This wire width $W \simeq 350$–450 Å agrees with the width one calculates by attributing the reduction in the zero-field conductance simply to a reduced cross-sectional area.[18]

For the two-dimensional electron gas in Fig. 3, formed when both gate voltages are large so that $V_{TG} = 13$ V and $V_{BG} = 3$ V, the two-terminal device conductance decreases with increasing magnetic field. This decreasing two-terminal current with increasing magnetic field is the same magnetoconductance as in a standard wide MOSFET device. As our grating gate device is pinched into long and narrow wires, such as when $V_{TG} = 13$ V and $V_{BG} = 0$ V in Fig. 3, there is almost no dependence of the background conductance on the magnetic field. All the curves display Shubnikov–de Haas oscillations, but the background magnetoconductance changes completely from a negative magnetoconductance in a wide device to almost no magnetoconductance in the narrow device. This difference is still further indication that narrow inversion channels are actually being formed. The curve having $V_{TG} = -7$ V and $V_{BG} = 3$ V in Fig. 3, for which the electrons are confined underneath the grating lines, shows a qualitatively similar magnetoconductance to the two previous curves for which the electrons are confined in the gap between the grating lines, $V_{TG} = 13$ V and $V_{BG} = 0$ V and -1.25 V in Fig. 3.

The different magnetoconductance of the wide and narrow MOSFET is manifested in a quite dramatic way when the magnetic field is held fixed and the inversion-layer geometry is varied with the two gates as in Fig. 4. We fix the bottom-gate voltage at $V_{BG} = 3$ V and vary the inversion-layer geometry with the top gate. The "break" or "kink" in the static I-V curve around $V_{TG} \simeq 0$ V becomes quite prominent as the magnetic field is increased. For $V_{TG} \leq 0$ V the current is almost independent of magnetic field, consistent with the magnetoconductance of the array of narrow wires in Fig. 3. However, when $V_{TG} \geq 0$ V, the current drops very strongly with increasing magnetic field, consistent with the magnetoconductance of a standard wide MOSFET device. The seemingly counterintuitive result in Fig. 4 is that, as more electrons are added to the device by increasing the top-gate voltage, the current actually decreases when a magnetic field is present. The decrease in the current is not small; a drop of more than two-thirds of the original current is observed at a magnetic field of 8 T in Fig. 4.

We argue that the region of the curve in Fig. 4 for which $V_{TG} \leq 0$ is where the electron gas is confined into narrow-inversion channels. The decreasing conductance with increasing gate voltage occurs when the electron gas first becomes continuous across the channel with a modulated density, and the conductance continues to decrease until a minimum conductance occurs near $V_{TG} \simeq 8$ V for $B = 8$ T. The conductance minimum should occur when the gate voltages create an unmodulated two-dimensional potential. The rising conductance when $V_{TG} \geq 8$ V occurs partially because more carriers are being added to the inversion layer, but mainly because the combi-

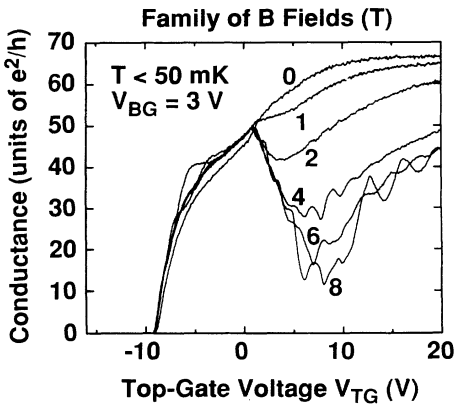

FIG. 4. A large negative transconductance appears near the kink at $V_{TG} = 0$ V in an applied perpendicular magnetic field of $B = 8$ T as the inversion-layer geometry opens from the narrow wire array into a two-dimensional electron gas. The additional carriers added to the inversion layer cannot overcome the decrease in the two-terminal current required by the new boundary conditions imposed on the Drude conductance tensor. The current switches to flow across the device at the Hall angle as the inversion-layer geometry is opened, resulting in a large drop in the current.

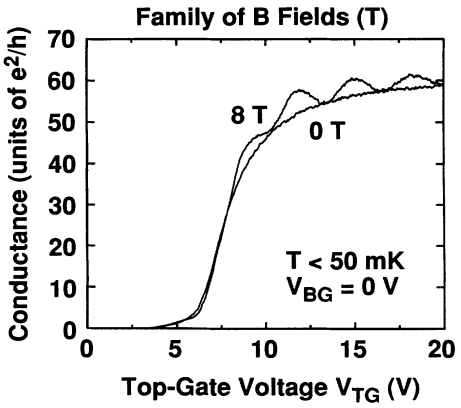

FIG. 5. For a device I-V curve from Fig. 1 having no kink, little or no background magnetoconductance is observed. This absence of substantial background magnetoconductance confirms that the electron gas exists only in the gap between grating lines, so that the inversion-layer geometry does not qualitatively change as the top-gate voltage is varied. The current path therefore continues to flow parallel to the side of the device irrespective of the magnetic field, producing little magnetoconductance.

nation of gate voltages now again produces a modulated potential.[19] On the rising part of the curve where $V_{TG} \geq 8$ V, the electrostatic potential minimum has now shifted over by half a grating period to lie in the gap between grating wires. (When 0 V$\leq V_{TG} \leq 8$ V on the falling part of the I-V curve, the electrostatic potential minimum lies underneath the grating gate wires.) A large negative transconductance similar to that in Fig. 4 can also be observed by fixing the top-gate voltage above its threshold and sweeping the bottom gate in an applied perpendicular magnetic field.

If our interpretation of Fig. 2 is correct, that the "breaks" in the device I-V curve correspond to an opening of the parallel narrow-inversion channels into a wide two-dimensional electron gas, then there should be very little magnetoconductance for bottom-gate voltages below threshold, $V_{BG} = 1$ V, 0 V, and -1 V, where there is no break in the static I-V. This is indeed the case as shown in Fig. 5, confirming that for this family of I-V curves the electron gas exists only in strips between the grating gate wires.

III. TEMPERATURE DEPENDENCE

To understand whether the large negative transconductance in Fig. 4 is a classical or a quantum-mechanical effect, we study its temperature dependence. Figure 6(a) shows the current on a different device when $V_{BG} = 3.5$ V. We sweep the top-gate voltage for temperatures $T = 4.2$ K, 20 K, 50 K, 100 K, 200 K, and 280 K. The total series resistance is 120 Ω in Fig. 6, since different measurement equipment is now being used. This different device and measurement setup is used in Figs. 6–9. Although fringing fields are able to shut off the device when $T = 4.2$ K, we see that by the time the device is at room temperature (280 K) the fringing fields are much less effective. We do not understand this difference in detail. The decrease in conductance with increasing temperature is presumably due to an increase in electron-phonon scattering with increasing temperatures.

The effect of a 15-T magnetic field normal to the Si-SiO_2 interface on these curves is shown in Fig. 6(b). The $T = 4.2$ K curve for $B = 0$ is also shown for comparison (dashed line). At $T = 4.2$ K and $B = 15$ T, a single Shubnikov–de Haas oscillation is observable over the range of gate voltages shown. By $T = 20$ K the Shubnikov–de Haas oscillation is no longer present, indicating that the Landau-level structure has completely deteriorated. Yet the large negative transconductance seen in Fig. 6(b) persists even to room temperature. We conclude that the effect is completely classical.

This classical magnetoconductance effect does not arise from confinement of the electrons to dimensions smaller than the cyclotron radius or mean free path. In this sample a generous estimate of the mean free path which enters the Drude conductance is roughly 600 Å when $T = 4.2$ K. Thus, the mean free path can be greater than the wire width at low temperature, but this does not seem possible at room temperature when the mean free path is 5–10 times smaller. Also, at a magnetic field of $B = 15$ T, the cyclotron radius in (100)

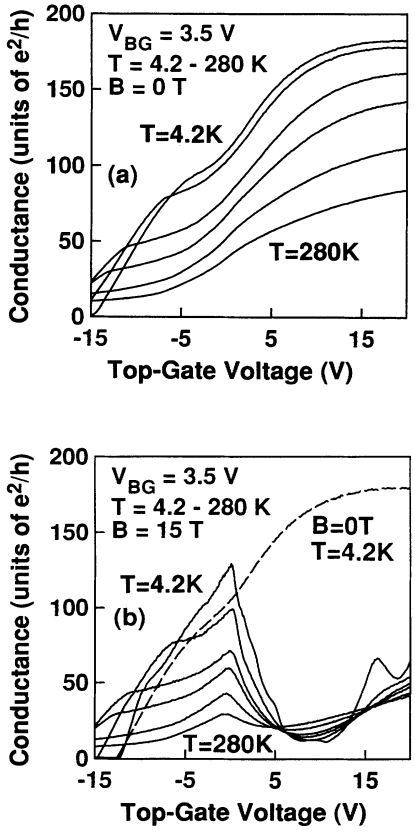

FIG. 6. Temperature dependence of the device current shown for $T = 4.2$ K, 20 K, 50 K, 100 K, 200 K, and 280 K. The magnetic field is (a) $B = 0$ T and (b) $B = 15$ T normal to the sample surface. The large negative transconductance in (b) persists to room temperature, confirming its classical origin.

Si is less than 100 Å, which is much smaller than the wire width, yet the observed negative transconductance becomes larger, not smaller, as the magnetic field is increased.

The correct explanation for the behavior of the magnetoconductance as the inversion layer geometry changes was provided by Park.[12] Assume the magnetoconductance is described by the Drude conductance tensor. This assumption is appropriate if the device is not in the quantum Hall limit so that local resistances can still be defined. One must obtain the two-terminal device conductance using the Drude tensor, by calculating the current consistent with the boundary conditions on the current and voltage. The boundary conditions are (1) that no current can flow through the side of the device, and (2) that the voltage at the source terminal be zero and at the drain terminal be V_{DS}, since the device contacts are heavily doped and can thus be approximated as an equipotential surface.

In a long and narrow geometry for which $L \gg W$, and well away from the device ends, the current distribution along the channel from one differential slice of the device to the next must be the same, as shown in Fig. 7(a). Therefore, the current mostly flows parallel to the edge of the device and the electric field is pointed away from the current path by the Hall angle. Since the current distribution is known, one can integrate

$$E_x = \rho_{xx} J_x + \rho_{xy} J_y \tag{1}$$

from source to drain. The term involving ρ_{xy} is completely negligible when $L \gg W$ (and $\rho_{xx} \neq 0$, i.e., the device is not in the quantum Hall limit) so one obtains the two-terminal resistance R_{2P} of the device as

$$R_{2P} \simeq L\rho_{xx}/W. \tag{2}$$

This result makes sense, as it is just the standard argument for measuring ρ_{xx} in a Hall bar geometry. To make an accurate measurement of ρ_{xx} in a Hall bar geometry one wishes to make a sample very long and narrow, and keep the Hall probes well away from the ends of the device. Equation (2) for the two-terminal resistance has been previously suggested by Syphers and Stiles.[20]

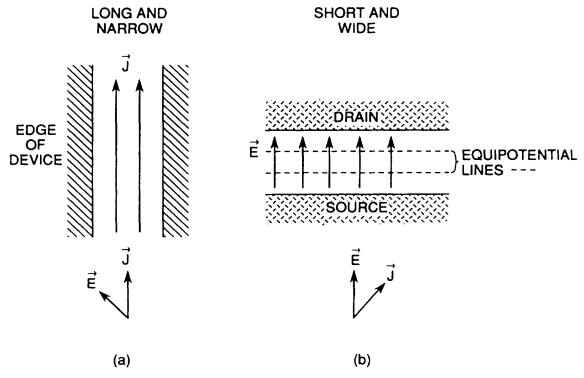

FIG. 7. To obtain the two-terminal conductance from the Drude conductance tensor, we apply boundary conditions on the current and electric field appropriate to the inversion-layer geometry. For (a) a long and narrow conductor, the current must continue to flow parallel to the side of the device even at moderate magnetic fields. If the conductor is (b) short and wide, the electric field points directly from source to drain and the current flows across the device at the Hall angle.

Conversely, in the short and wide geometry of Fig. 7(b) for which $W \gg L$, the edges of the device are far away so that the current will have to adjust to the boundary condition on the voltage. For the short and wide geometry, the equipotential surfaces must be the same as one moves laterally across the channel as in Fig. 7(b). Therefore, the electric field points directly from source to drain and the current flows at the Hall angle across the channel. There are minor corrections to this picture at the edges of the device, which are small if $W \gg L$. Consequently, since the electric field is known, the two-terminal current can be obtained by integrating

$$J_x = \sigma_{xx} E_x + \sigma_{xy} E_y \tag{3}$$

from source to drain. One obtains in the limit $W \gg L$ and $\sigma_{xx} \neq 0$, where the second term in Eq. (3) is negligible, that the two-terminal conductance G_{2P} is

$$G_{2P} \simeq W\sigma_{xx}/L \tag{4}$$

Reference 21 has suggested a similar expression for the two-terminal magnetoconductance of a short and wide conductor.

The classical Eq. (2) and Eq. (4) qualitatively explain the data in Fig. 4. Since ρ_{xx} is independent of magnetic field, Eq. (2) predicts that in a long and narrow device where $L \gg W$ there is no magnetoconductance. Conversely, since σ_{xx} varies with magnetic field as $1/[1 + (\mu B)^2]$, where μ is the electron mobility and B the magnetic field, the two-terminal conductance of a short and wide device where $W \gg L$ decreases as the magnetic field increases. Fitting the two-terminal conductance from Fig. 3 for $V_{TG} = 13$ V and $V_{BG} = 3$ V to the form $G = G_0/[1 + (\mu B)^2]$ gives an electron mobility $\mu \simeq 4000$ cm^2/V s after series resistance correction. This mobility is the same order of magnitude as the measured field-effect mobility, and gives additional support to Eq. (4). To explain completely the data in Fig. 4, such as the conductance minima occuring at different values of V_{TG} for different values of the magnetic field, one needs a theory of classical magnetoconductance in a modulated potential which is not available at this time. However, Eqs. (2) and (4) qualitatively explain most of the data. The large negative transconductance observed in Fig. 4, and the difference between Eqs. (2) and (4), arises because the current switches direction to flow across the device at the Hall angle as the inversion layer geometry is opened electrostatically.

How Eqs. (2) and (4) relate to more complicated expressions[22,23] for the two-terminal magnetoconductance in terms of the conductance tensor elements is not clear. One would expect to obtain Eqs. (2) and (4) from Refs. 22 and 23 in the appropriate limits. Park[12] has constructed a proof using the conformal mapping technique of Ref. 22 that there is a symmetry between G_{2P} in the $W \gg L$ limit and R_{2P} in the $L \gg W$ limit. As a

special case, this symmetry implies that, if Eq. (2) holds in the limit of $L \gg W$, then Eq. (4) holds when $W \gg L$.

IV. HIGH MAGNETIC FIELDS

We turn to the behavior of the conductance at large magnetic fields. Figure 8 shows the conductance (corrected for series resistance) when $V_{BG} = 3.5$ V and the top gate is swept between -15 V $\leq V_{TG} \leq 25$ V for a family of magnetic fields $B = 0$ T, 5 T, 10 T, 15 T, 20 T, and 23 T at a temperature $T = 1.2$ K. For top gate voltages $V_{TG} \geq 5$ V, the inversion layer forms a short and wide conductor (right side of Fig. 8). In this short and wide geometry, the high-field conductance continues to decrease with the large applied magnetic field. Thus, neglecting the appearance of Shubnikov–de Haas oscillations in the conductance, the high-field magnetoconductance for the short and wide geometry has the same sign as the classical Drude magnetoconductance at moderate magnetic fields. For top gate voltages $V_{TG} \leq 0$ V, the inversion-layer geometry consists of many parallel long and narrow conductors (left side of Fig. 8). When the electrons are confined to these long and narrow conductors, the current remains roughly constant up to a magnetic field of 15 T as before. Thus, neglecting again the appearance of Shubnikov–de Haas oscillations, the background magnetoconductance lies roughly in the classical Drude regime to about 15 T. But in contrast to our previous results at low magnetic fields, for the magnetic field values of 20 T and 23 T, there is an additional large increase in the current in the long and narrow conductors at high magnetic fields. Thus, the high-field magnetoconductance has an opposite sign on different parts of the same device curve in Fig. 8, corresponding to either a high- or low-aspect-ratio conductor.

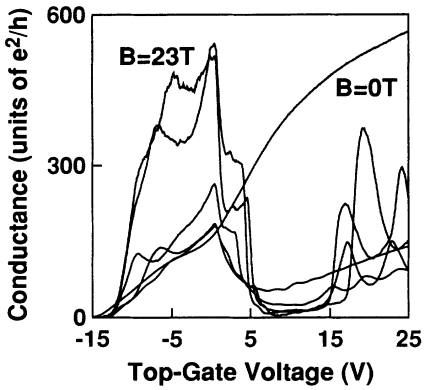

FIG. 8. Conduction in a large magnetic field having values $B = 0$ T, 5 T, 10 T, 15 T, 20 T, and 23 T at a temperature $T = 1.2$ K. The bottom gate is held at $V_{BG} = 3.5$ V. For the long and narrow conductors formed below $V_{TG} = 0$ V on the left side of the figure, there is a large increase in the current at the two highest values of the magnetic field. This large positive magnetoconductance indicates the formation of quantum edge states and the approach to the quantum Hall effect. The approach to the quantum Hall effect is qualitatively different when the inversion layer geometry is short and wide (above $V_{TG} = 5$ V on the right of the figure), where the high-field magnetoconductance is negative. This is also explained by quantum edge-state formation.

We claim that this additional increased conductance in the long and narrow wires is due to edge states forming in the wire array as outlined by Büttiker.[24] Our device is 60 μm wide and the grating period is 0.2 μm, so that roughly 300 wires are present in the array. In a high magnetic field each wire must have a conductance of $2e^2/h$, the same conductance as that in a quantum ballistic conductor.[25] Since the wires have many scattering centers, their initial conductance at zero field is much less than the ballistic value. Therefore the conductance must rise with magnetic field when edge states begin to be formed in the wire, giving a conductance of $2e^2/h$ times the number of wires in parallel. The conductance of the wide MOSFET will also approach $2e^2/h$ at large magnetic fields. But since many conduction channels are initially occupied in the wide MOSFET, so that its total two-terminal conductance is much larger than $2e^2/h$ when $B = 0$, its conductance must continue to fall at large magnetic fields to approach the quantum Hall conductance limit. Therefore, depending on whether conduction occurs in many parallel narrow wires or a two-dimensional MOSFET, the high-field magnetoconductance must change sign as the device aspect ratio changes from long and narrow (positive magnetoconductance) to short and wide (negative magnetoconductance).

To prove that edge-state conduction is occurring, we measured the conductance of electrons confined in the gap between grating lines where $V_{BG} = 0$ V and $B = 0$ T, 10 T, 20 T, and 30 T. The results are shown in Fig. 9 (corrected for series resistance). For $B = 0$ T and 10 T, the current versus top-gate voltage qualitatively resembles Fig. 5, where Shubnikov–de Haas oscillations appear in the conductance and the background magnetoconductance is flat. When $B = 30$ T a well-defined quantum Hall plateau develops at $1200e^2/h$, with weaker precursors to quantum Hall plateaus appearing near $600e^2/h$ and $1800e^2/h$. Quantum Hall plateaus were reported in the two-terminal conductance by Fang and Stiles,[26] and fit nicely with the theory developed by Büttiker.[24] Since the device has 300 parallel wires, we interpret the Hall plateau at $1200e^2/h$ as the first filled Landau level with spin and valley degeneracy, due to the two conduction-band valleys at a (100) Si surface. Note, however, that only one of the degeneracies (at $600e^2/h$) is resolved in the conductance. Following Refs. 11–13 and 27, we interpret this as evidence that the valley degeneracy is restored in the wire.[27]

We feel that the large magnetic field of 30 T required to observe the quantum Hall effect in this sample is due partially to a lower sample mobility, but also to the fact that for such a narrow channel only a single impurity is required to destroy the quantization. Also, the quantized Hall conductance is more difficult to observe in a two-terminal measurement, where electrons must travel between two highly disordered contacts, than in a standard Hall bar geometry where they travel only along a relatively clean sample edge in the region of interest. This may also help to explain why such a large magnetic field

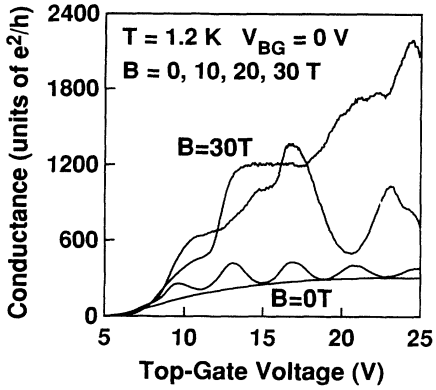

FIG. 9. Two-terminal conductance of a narrow wire array in an applied magnetic field of $B = 0$ T, 10 T, 20 T, and 30 T. Shubnikov–de Haas oscillations are seen when $B = 10$ T, and quantum Hall plateaus appear when $B = 30$ T. The wide Hall plateau at $1200e^2/h$ is formed by the 300 parallel wires having their lowest fourfold degenerate Landau level filled.

is required to obtain the quantized two-terminal conductance in Fig. 9.

The magnetic field value $B = 20$ T is an intermediate case between the Shubnikov–de Haas oscillations and the quantum Hall effect. This curve, showing the evolution from Shubnikov–de Haas oscillations to the quantum Hall effect in a narrow conductor, reproduces qualitatively the phenomenology observed by Kastner *et al.*[11] in narrow MOSFET's. The anomalous filling factors in Ref. 11 have since been explained[12] in a model which takes into account how edge states form in the various thick and thin oxide regions underneath the gate for the samples in Ref. 11. In our present device the narrow wire runs straight between the three-dimensional degenerately doped source and drain, and not through any two-dimensional regions or under different gate oxide thicknesses.

V. CONCLUSION

We originally undertook this study in an effort to see some manifestation of quasi-one-dimensional subbands in the device conductance[1,2,28–30] in a diffusive sample. This was not observed in these particular devices even though the wire width was shown to be much smaller than the electron phase coherence length. However, a variety of magnetoresistance effects were studied. Weak localization at low values of the magnetic field was found to become a much stronger effect in the conductance, and to persist to a much larger value of magnetic field, when the electron gas is pinched into a wire narrower than the phase coherence length. This modification to weak localization is the only magnetoconductance effect studied here that depends on the extreme narrowness of the quantum wire. The two other magnetoconductance effects studied, the different background magnetoconductance at moderate fields and different approaches to the quantum Hall effect at high fields, depend primarily on the aspect ratio of the conductor (long and narow versus short and wide) and not on the conductor being narrower than the phase coherence length. The grating gate enabled us to directly compare the magnetoresistance of a two-dimensional sample with multiple parallel one-dimensional conductors, since the conductance of both systems are the same order of magnitude and can be displayed on the same graph.

We also observed that the two-terminal Drude magnetoconductance of an inversion layer is strongly determined by the device aspect ratio (when a local magnetoconductance tensor description of conduction is appropriate). This is in contrast to the two-terminal resistance of a quantum Hall conductor, in which the resistance is independent of the size and shape of the conductor. A long and narrow conductor was found to have very little dependence of the two-terminal resistance on magnetic field, while a short and wide conductor has a two-terminal resistance which increases with magnetic field. This difference is manifested as a large negative transconductance (a decrease in the current as more electrons are added to the device) of our grating gate MOSFET when the magnetic field is held fixed and the device geometry is opened electrostatically from many narrow wires in parallel into a two-dimensional conductor. As the inversion-layer geometry is opened electrostatically, the current direction switches from flowing directly from source to drain (long and narrow conductor) to flow at the Hall angle across the device (short and wide conductor), producing the large negative transconductance observed in this study.

Finally, for conduction in very high magnetic fields, the magnetoconductance was shown to have opposite sign for the multiple parallel narrow wires and the two-dimensional MOSFET. Therefore, the evolution from the Drude magnetoconductance to the Shubnikov–de Haas oscillations and quantum Hall effect depends strongly and qualitatively on the device aspect ratio. The long and narrow wire (with a zero-field conductance much less than $2e^2/h$) must suffer an increase in conductance at high magnetic fields, while the short and wide channel (with a zero-field conductance much greater than $2e^2/h$) must become less conductive at high magnetic fields. We interpret this result in terms of magnetic quantum edge-state formation in the wire array, as confirmed by the appearance of quantum Hall plateaus at the highest magnetic fields. Again, this result depends primarily on the device aspect ratio and not the narrowness of the wires. The observed quantum Hall steps have size $2e^2/h$ since the conduction-band valley degeneracy is not resolved.

ACKNOWLEDGMENTS

We thank John Scott-Thomas, Udi Meirav, Norris Preyer, Seiji Horiguchi, and Akira Toriumi for experimental help. The high-magnetic-field measurements were carried out at the MIT Francis Bitter National Magnet Laboratory, which is supported by the National Science Foundation. We thank Larry Rubin, Bruce Brandt, and

Jing Luo for assistance with the high-magnetic-field measurements. James Carter, Mark Schattenburg, and the staff at the MIT Submicron Structures Laboratory and MIT Microsystems Technology Laboratories greatly assisted in device fabrication. This work was sponsored by the U.S. Joint Services Electronics Program Contract No. DAAL03-89-C-0001 and the U.S. Air Force Office of Scientific Research under Grant No. AFOSR-88-0304.

---

*Present address: Department of Electrical Engineering, Purdue University, West Lafayette, Indiana 47907.

†Present address: Institute for Defense Analyses, 1801 N. Beauregard Street, Alexandria, Virginia, 22311.

‡Present address: Texas Instruments, Semiconductor Process and Design Center, P.O. Box 655012, MS 944, Dallas, Texas 75265.

[1] A.C. Warren, D.A. Antoniadis, and H.I. Smith, Phys. Rev. Lett. **56**, 1858 (1986).

[2] J.R. Gao, C. de Graaf, J. Caro, S. Radelaar, M. Offenberg, V. Lauer, J. Singleton, T.J.B.M. Janssen, and J.A.A.J. Perenboom, Phys. Rev. B **37**, 6181 (1990).

[3] J.H.F. Scott-Thomas, M.A. Kastner, D.A. Antoniadis, H.I. Smith, and S.B. Field, J. Vac. Sci. Technol. B **6**, 1841 (1988).

[4] J.H.F. Scott-Thomas, S.B. Field, M.A. Kastner, H.I. Smith, and D.A. Antoniadis, Phys. Rev. Lett. **62**, 583 (1989).

[5] A. Yen, S.M. thesis, Massachusetts Institute of Technology, 1987.

[6] A.B. Fowler, A. Hartstein, and R.A. Webb, Phys. Rev. Lett. **48**, 196 (1982).

[7] M. Pepper and M.J. Uren, J. Phys. C **15**, L617 (1982).

[8] W.J. Skocpol, P.M. Mankiewich, R.E. Howard, L.D. Jackel, and D.M. Tennant, Phys. Rev. Lett. **56**, 2865 (1986).

[9] M.A. Kastner, R.F. Kwasnick, J.C. Licini, and D.J. Bishop, Phys. Rev. B **36**, 8015 (1987).

[10] C.C. Dean and M. Pepper, in *Proceedings of the 17th International Conference on the Physics of Semiconductors*, edited by D.J. Chadhi and W.A. Harrison (Springer-Verlag, Berlin, 1984), p. 425.

[11] M.A. Kastner, S.B. Field, J.C. Licini, and S.L. Park, Phys. Rev. Lett. **60**, 2535 (1988).

[12] S.L. Park, Ph.D. thesis, Massachusetts Institute of Technology, 1990.

[13] A.B. Fowler, A. Hartstein, and R.A. Webb, Physica **117B&118B**, 661 (1983).

[14] C.C. Dean and M. Pepper, in *Localization, Interaction, and Transport Phenomena*, edited by B. Kramer, G. Bergmann, and Y. Bruynseraede (Springer-Verlag, Berlin, 1985).

[15] The small conductance which is independent of the top-gate voltage on these three curves, $V_{BG} = 1$ V, 0 V, and -1 V in Fig. 2, arises from a parasitic parallel current path around the side of the device. This additional current path does not significantly alter the data we present. For example, it can be seen from Fig. 2 that the parasitic current path does not begin to conduct until $V_{TG} = 5$ V, and even then is not a significant fraction of the total current for the values of gate voltages shown in the remaining figures. Further, since the parasitic path has a high aspect ratio (longer than its width), it has little Drude magnetoresistance of its own, as can be confirmed from Fig. 5. The high-field magnetoresistance of the parasitic current path is similar to the long and narrow MOSFET.

[16] G. Bergman, Phys. Rep. **107**, 1 (1984).

[17] B.L. Al'tshuler and A.G. Aronov, Pis'ma Zh. Eksp. Teor. Fiz. **33**, 515 (1981) [JETP Lett. **33**, 499 (1981)].

[18] If only 400 Å of each 2000-Å grating period conduct, the zero-field conductance should decrease by a factor of 5 as the device is pinched into many narrow wires in parallel. This factor of roughly 5 is not seen directly in Fig. 3 because series resistance limits the measured conductance.

[19] These points must be considered tentative, as an explicit solution for classical transport in a modulated potential which properly incorporates the device boundaries is not available.

[20] D.A. Syphers and P.J. Stiles, Phys. Rev. B **32**, 6620 (1985).

[21] J.P. Harrang, R.J. Higgins, R.K. Goodall, P.R. Jay, M. Laviron, and P. Delescluse, Phys. Rev. B **32**, 8126 (1985).

[22] R.W. Rendell and S.M. Girvin, Phys. Rev. B **23**, 6610 (1981).

[23] G.L.J.A. Rikken, J.A.M.M. van Haaren, W. van der Wel, A.P. van Gelder, H. van Kempen, P. Wyder, J.P. Andre, K. Ploog, and G. Weimann, Phys. Rev. B **37**, 6181 (1988).

[24] M. Büttiker, Phys. Rev. B **38**, 9375 (1988).

[25] B.J. van Wees, H. van Houten, C.W.J. Beenakker, J.G. Williamson, L.P. Kouwenhoven, D. van der Marel, C.T. Foxon, Phys. Rev. Lett. **60**, 848 (1988); D.A. Wharam, T.J. Thornton, R. Newbury, M. Pepper, H. Ahmed, J.E.F. Frost, D.G. Hasko, D.C. Peacock, D.A. Ritchie, and G.A.C. Jones, J. Phys. C **21**, L209 (1988).

[26] F.F. Fang and P.J. Stiles Phys. Rev. B **27**, 6487 (1983).

[27] J.M. Kinaret and P.A. Lee, Phys. Rev. B **42**, 11 768 (1990).

[28] K. Ismail, D.A. Antoniadis, and H.I. Smith, Appl. Phys. Lett. **54**, 1130 (1989).

[29] K. Ismail, S. Washburn, and K.Y. Lee (unpublished).

[30] A. Kumar and P.F. Bagwell, Phys. Rev. B **44**, 1747 (1991).